Vanadium Oxide–PANI Nanocomposite-Based Macroscopic Fibers: 1D Alcohol Sensors Bearing Enhanced Toughness

ARTICLE *in* CHEMISTRY OF MATERIALS · AUGUST 2008

Impact Factor: 8.35 · DOI: 10.1021/cm800886v

Vanadium Oxide−PANI Nanocomposite-Based Macroscopic Fibers: 1D Alcohol Sensors Bearing Enhanced Toughness

J. Dexmer,[†] C. M. Leroy,[†] L. Binet,[‡] V. Heresanu,[§] P. Launois, N. Steunou,*[,||] C. Coulon,[†] J. Maquet,[‡] N. Brun,[†] J. Livage,[||] and R. Backov*[,†]

Centre de Recherche Paul Pascal, Office 115, UPR 8641-CNRS, 115 Avenue Albert Schweitzer, 33600 Pessac, France, Laboratoire de Chimie de la Matière Condensée de Paris, UMR-7574 CNRS, Ecole Nationale Supérieure de Chimie de Paris, 11 rue Pierre et Marie Curie, 75005 Paris France, Laboratoire de Physique des Solides, UMR-CNRS 8502, Bât. 510, Université Paris Sud, 91405 Orsay, France, Laboratoire de Chimie de la Matière Condensée de Paris, UMR-7574 CNRS, Collège de France, UPMC, Univ Paris 06, 4 Place Jussieu, 75252 Paris Cedex 05, France

Received March 27, 2008. Revised Manuscript Received July 1, 2008

For the first time, using an extrusion process, macroscopic composite poly-vinyl alcohol(PVA)/polyaniline (PANI)-V_2O_5 fibers have been generated. Besides the extrusion process itself, this is certainly the first redox reaction addressed while performing an extrusion shaping process. The as-synthesized fibers have been characterized at different length scales, revealing at the mesoscale a 30° preferential orientation of the nanoribbons subunits toward the macroscopic fiber main axis. At the microscopic length scale, despite a semiamorphous nature, electron spin resonance (ESR) spectroscopy has been employed to reveal partial reduction of V^{5+} species to V^{4+} ones, where the paramagnetic species local environment has been found to be close to hydrated vanadium oxide xerogels. Concerning the organic counterpart, the aniline is oxidized into poly aniline when considering both the fibers characterization through ESR and Fourier transformed infrared (FTIR) spectroscopy and the well-known strongly oxidizing character of V^{5+} species toward aniline. These new PVA/PANI-V_2O_5 fibers are cycling when sensing alcoholic vapors while offering a good selectivity. The addressed sensitivity allows sensing 5 ppm of ethanol within 3−5 s at 42 °C. Beyond, the as-synthesized PVA/PANI-V_2O_5 macroscopic fibers possess a toughness of 12 J g^{-1}, a value that has been increased by more than 120 times when compared with nanoporous inorganic fibers.

Introduction

Recently, the new transversal concept of "integrative chemistry" has been postulated as a versatile pathway to design and engineer functional architectures, where chemistry, physical chemistry of complex fluids, and biology appear as specific items to compose their own synthetic route to reach specific multiscale architectures bearing functionalities acting in registry or not.[1] Syntheses over "all length scales"[2] and/or bioinspired approaches[3,4] were proposed around 15 years ago by G. Ozin and S. Mann, respectively, with a strong scientific echo mainly due to both the understanding insights toward complex chemical reactions occurring at the organic−inorganic interface and final contemplative issues of the as-synthesized architectures.[2−4] Integrative chemistry, through an engineered-synthetic pathway, has been already widely applied by combining general chemistry with foams,[5] emulsions,[6] lyotropic mesophases,[7] biologic polymer,[8] three-dimensional colloid opal-like textures,[9] and more recently with millifluidic.[10] To the previous set of texturing modes that mostly regard the areas of soft matter, we might combine inorganic polymerization occurring under soft conditions, namely, "soft chemistry".[11] More precisely, the sol−gel process[12] appears as a candidate of

* Corresponding author. Phone: 33 (0)5 56 84 56 30 (R.B.); 33 (0)1 44 27 55 45 (N.S.). Fax: 33 (0)5 56 84 56 00 (R.B.); 33 (0)1 44 27 47 69 (N.S.). E-mail: backov@crpp-bordeaux.cnrs.fr (R.B.); nathalie.steunou@upmc.fr (N.S.).
[†] Centre de Recherche Paul Pascal.
[‡] Ecole Nationale Supérieure de Chimie de Paris.
[§] Université Paris Sud.
[||] Collège de France.

(1) Backov, R. *Soft Matter* **2006**, *2*, 452.
(2) (a) Yang, H.; Kuperman, A.; Coombs, N.; Mamiche-Afara, S.; Ozin, G. A. *Nature* **1996**, *379*, 703. (b) Feng, P.; Bu, X.; Stucky, G. D.; Pine, D. J. *J. Am. Chem. Soc.* **2000**, *5*, 994.
(3) (a) Mann, S. *Nature* **1988**, *332*, 119. (b) Archibald, D. D.; Mann, S. *Nature* **1993**, *364*, 430.
(4) Xu, A.-W.; Ma, Y.; Cölfen, H. *J. Mater. Chem.* **2007**, *5*, 415.
(5) (a) Carn, F.; Colin, A.; Achard, M.-F.; Deleuze, H.; Backov, R. *Adv. Mater.* **2004**, *16*, 140. (b) Carn, F.; Colin, A.; Achard, M.-F.; Deleuze, H.; Sanchez, C.; Backov, R. *Adv. Mater.* **2005**, *17*, 62. (c) Carn, F.; Steunou, N.; Livage, J.; Colin, A.; Backov, R. *Chem. Mater.* **2005**, *17*, 644.
(6) (a) Imhof, A.; Pine, D. J. *Nature* **1997**, *389*, 948. (b) Schacht, S.; Huo, Q.; Voigt-Martin, I. G.; Stucky, G. D.; Schüth, F. *Science* **1996**, *273*, 768. (c) Carn, F.; Colin, A.; Achard, M.-F.; Sellier, E.; Birot, M.; Deleuze, H.; Backov, R. *J. Mater. Chem.* **2004**, *14*, 1370. (d) Fornasieri, G.; Badaire, S.; Backov, R.; Mondain-Monval, O.; Zakri, C.; Poulin, P. *Adv. Mater.* **2004**, *16*, 1094.
(7) Jung, J. H.; Yoshiyuki, Y.; Shinkai, S. *Angew. Chem., Int. ed.* **2000**, *39*, 1862.
(8) Hall, S. R.; Bolger, H.; Mann, S. *Chem. Commun.* **2003**, 2784.
(9) Wang, D.; Caruso, R. A.; Caruso, F. *Chem. Mater.* **2001**, *13*, 364.
(10) (a) Tachibana, M.; Engl, W.; Panizza, P.; Deleuze, H.; Lecommandoux, S.; Ushiki, H.; Backov, R. *Chem. Eng. Process.* **2008**, *47*, 1323. (b) Engl, W.; Tachibana, M.; Panizza, P.; Backov, R. *Int. J. Mult. Flow* **2007**, 897. (c) Panizza, P.; Engl, W.; Hany, C.; Backov, R. *Colloids Surf., A* **2008**, *312*, 24.
(11) Livage, J. *New J. Chem.* **2001**, *25*, 1.
(12) (a) Brinker, C. J.; Scherer, G. W. In *Sol−Gel Science: The Physics and Chemistry of Sol−Gel Processing*; Academic Press: San Diego, 1990. (b) Livage, J. *Chem. Mater.* **1991**, *3*, 578.

10.1021/cm800886v CCC: $40.75
Published on Web 08/13/2008

choice to both promote inorganic connectivity while not destroying the templates in use at different length scales. Particularly, vanadium oxide is of strong interest as associated with versatile properties ranging from catalysis to photochromism and so forth.[13] Gels of vanadium oxide can be obtained from sodium metavanadate as inorganic precursor and upon a ion exchange process where the final texture is composed of vanadium oxide nanoribbon subunits bearing strong anisotropy[14,12b] and allows generating a inorganic liquid crystal associated with a nematic character.[15] We first took benefit of this textural property by aligning the ribbon subunits with the use of an extrusion process, generating the first macroscopic fibers made of vanadium oxide with specific alcohol sensors properties;[16] later on, by varying the shear rate applied to the gel during the extrusion process, we were able to tune both the as-synthesized fibers' mechanical and sensing properties.[17] More recently, by varying the starting latex inclusion contents and the shear rates applied during the extrusion process and by performing a thermal treatment, we were able to segregate each parameter involved within the fibers mechanical and sensing properties, as the amount of the organic-insulator counterpart, the degree of vanadium oxide ribbon alignment, and the induced porosity reached upon latex removal. Overall, we found that all the parameters described above and involved within the as-synthesized fibers mechanical and sensing properties are acting within a partitive action mode rather than a cooperative one.[18] With this last study, we concluded that a nice way to promote and enhance both the fiber sensing and mechanical properties would be to generate an extrinsic plasticity associated with an intrinsic enhanced conductivity. To reach the above specificity, we took inspiration from earlier work[19] that reported the synthesis of hybrid compounds made of conducting polymers intercalated within V_2O_5 lamellae for the design of positive electrodes for lithium batteries. It has been evidenced that such composites can exhibit better specific capacity, redox cyclability and structural stability than the organic or inorganic components alone. Particularly, the conductivity of V_2O_5/PANI nanocomposite can be 1×10^4 higher than the V_2O_5 one. On the other hand, most of the studied conducting polymers/V_2O_5 hybrids are not particularly organized at the nano- or mesoscopic length scales. In this study we combine the introduction of a functional conducting polymer enable to enhance both the electrical conductivity and the mechanical properties with an extrusion process that favors a structuration of the material from the mesoscopic to the macroscopic length scales.

Experimental Section

Materials. Dowex 50WX2−100 ion-exchange resin, sodium metavanadate (90%), polyvinyl alcohol (hydrolyzed 87−89%) and aniline were purchased from Aldrich. All materials were used as received whithout further purification.

Syntheses. Synthesis of V_2O_5, nH_2O gels was performed by the classical ion exchange method.[12b,14] A solution of a sodium metavanadate ($NaVO_3$) precursor of concentration 0.1 mol/L is passed through a proton exchange resin (DOWEX-W-hydrogen, strongly acid cationic, 2% cross-linking 50−100 mesh). While acidification occurs, the pH of the solution decreases from 7 to 2.6. At a pH close to 2, the solution starts to polymerize and after 20 h, a dark red gel of V_2O_5 ribbons is formed. The vanadium weight fraction of this gel was determined by preparing a dry extract. Solutions suitable for the extrusion process have been made by mixing 3.85 g of the starting vanadium oxide gel with 6.15 g of dimethylsulfoxide (DMSO) to reach 1.2 wt % vanadium oxide sol. The vanadium oxide fibers were obtained by extruding a 1.2 wt % vanadium oxide aqueous/DMSO sol into a water/DMSO (50/50 % vol) solution containing 2 wt % polyvinyl alcohol (PVA) and 7 wt % aniline. The beaker containing the PVA−aniline solution is kept at constant rotation speed of 50 rotations per minutes (rpm) while the vanadium oxide gel was extruded out of its containing syringe at the 50 mL/h constant low flux. Upon extrusion process completion, the vanadium oxide threads were meticulously taken out of beaker by hand and let to dry in air. Finally the as-synthesized fibers were washed three times in THF/acetone (50 vol %) for a 1 day period and then let to dry in air.

Characterization. Final inorganic fibers were then analyzed. Scanning Electron Spectroscopy (SEM) observations were performed with a JEOL JSM-840A scanning electron microscope operating at 10 kV. The specimens were carbon-coated prior examination. X-ray scattering experiments (SAXS) were performed using a rotating copper anode generator. Cu $K\alpha$ wavelength ($\lambda =$ 1.5418Å) was selected using a doubly bent graphite monochromator. Individual fibers were suspended on off-centered supports, so that no sample holder diffusion could pollute the measurements. Fiber long axis was perpendicular to the X-ray beam. The experiments were performed under vacuum to minimize air scattering and thus optimize the signal/background ratio. The data were recorded in transmission on an Image Plate. Small to wide angle data were recorded by varying the Image Plate to sample distance (from 150 to 25 mm). ^{51}V magic-angle spectroscopy nuclear magnetic resonance (^{51}V MAS NMR) spectra were recorded at 105.2 MHz on a Bruker Avance 400 spectrometer using a MAS 4 mm ^{1}H/BB probe. Vanadium oxide fibers were cut and packed in 4 mm ZrO_2 rotors. Solid samples were spun at 12.5 kHz. ^{51}V MAS NMR spectra were acquired with a rotor synchronized echo sequence ($\theta-\tau-2\theta-\tau-$acq. with $\theta = \pi/16$, $\tau = 1/\nu_r$, where ν_r is the spinning frequency) and with power levels corresponding to $\pi/2$ lengths for the liquid standard (NH_4VO_3) of approximately 2.5 μs. A spectral width of 2 MHz and a recycle delay of 0.5 s were used. The electronic scanning resonance (ESR) spectra were recorded at room

(13) (a) Baker, L. C. W.; Glick, D. C. *Chem. Rev.* **1998**, *98*, 3. (b) Hagrman, P. J.; Finn, R. C. O.; Zubieta, J. *J. Solid State Sci.* **2001**, *3*, 745.
(14) (a) Zöcher, H. *Z. Anorg. Allg. Chem.* **1925**, *147*, 91. (b) Lemerle, J.; Nejem, L.; Lefebvre, J. *J. Inorg. Nucl. Chem.* **1980**, *42*, 77.
(15) (a) Pelletier, O.; Davidson, P.; Bourgaux, C.; Livage, J. *Prog. Colloid Polym. Sci.* **1999**, *112*, 121. (b) Commeinhes, X.; Davidson, P.; Bourgaux, C.; Livage, J. *Adv. Mater.* **1997**, *9*, 900.
(16) Biette, L.; Carn, F.; Maugey, M.; Achard, M.-F.; Maquet, J.; Steunou, N.; Livage, J.; Serier, H.; Backov, R. *Adv. Mater.* **2005**, *17*, 2970.
(17) Serier, H.; Achard, M.-F.; Steunou, N.; Maquet, J.; Livage, J.; Leroy, C. M.; Babot, O.; Backov, R. *Adv. Funct. Mater.* **2006**, *16*, 1745.
(18) Leroy, C. M.; Achard, M.-F.; Babot, O.; Steunou, N.; Mass, P.; Livage, J.; Binet, L.; Brun, N.; Backov, R. *Chem. Mater.* **2007**, *19*, 3988.
(19) (a) Kanatzidis, M. G.; Wu, C.-G.; Marcy, H. O.; Kannewurf, C. R. *J. Am. Chem. Soc.* **1989**, *111*, 4139. (b) Wu, C.-G.; DeGroot, D. C.; Marcy, H. O.; Schindler, J. L.; Kannewurf, C. R.; Liu, Y.-J.; Hirpo, W.; Kanatzidis, M. G. *Chem. Mater.* **1996**, *8*, 1992. (c) Leroux, F.; Koene, B. E.; Nazar, L. F. *J. Electrochem. Soc.* **1996**, *143*, L181. (d) Gomez-Romero, P. *Adv. Mater.* **2001**, *13*, 163. (e) Posudievsky, O. Y.; Biskulova, S. A.; Pokhodenko, V. D. *J. Mater. Chem.* **2004**, *14*, 1419.
(20) (a) Pelletier, O.; Davidson, P.; Bourgaux, C.; Coulon, C.; Regnault, S.; Livage, J *Langmuir* **2000**, *16*, 5295. (b) Vigolo, B.; Zakri, C.; Nallet, F.; Livage, J.; Coulon, C. *Langmuir* **2002**, *18*, 9121.
(21) (a) Minus, M. L.; Chae, H. G.; Kumar, S. *Polymer* **2006**, *47*, 3705. (b) Meng, L.-J.; Silva, R. A.; Cui, H.-N.; Teixeira, V.; dos Santos, M. P.; Xu, Z. *Thin solid films* **2006**, *515*, 195. (c) Pichot, V.; Badaire, S.; Albouy, P. A.; Zakri, C.; Poulin, P.; Launois, P. *Phys. Rev. B* **2006**, *74*, 245416.

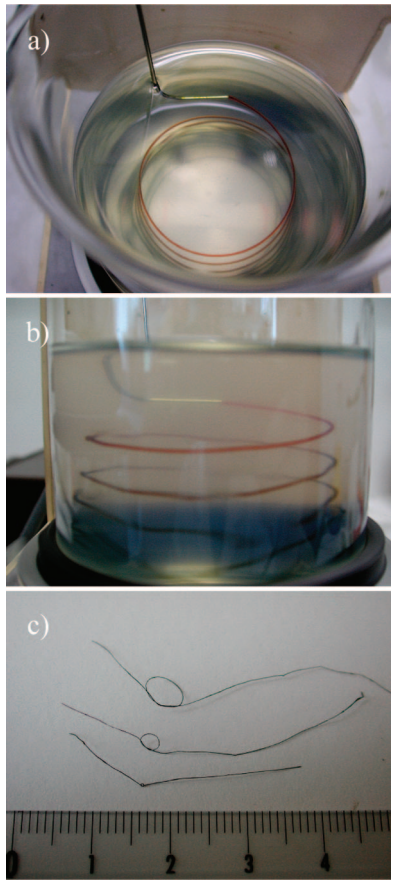

Figure 1. Experimental setup allowing the fiber extrusion: (a) top view of the rotating beaker, (b) side view of the rotating beaker, (c) several dried fibers forming knots.

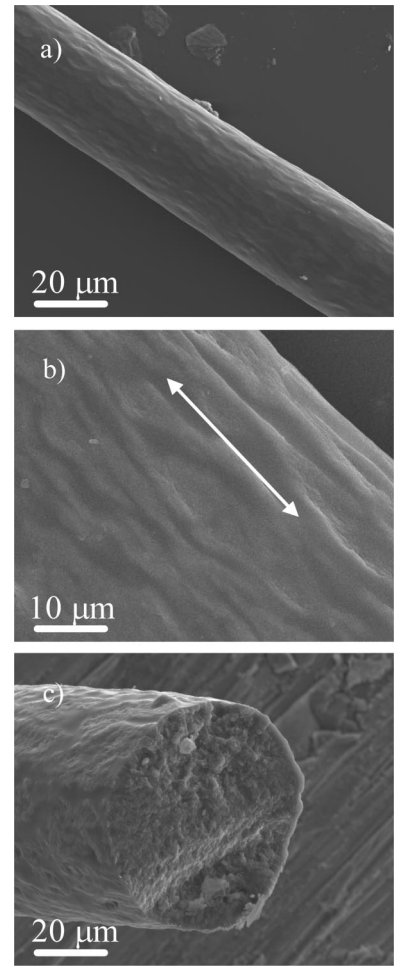

Figure 2. SEM pictures of fibers obtained with an applied shear rate γ of 235 s^{-1}: (a) transversal view, (b) picture focused on the texture of the fiber surface, (c) fiber section. The double white arrow indicates the fiber main axis.

temperature on a Bruker Elexsys E500 spectrometer operating at X band (9.4 GHz) equipped wit a SHQ cavity. A modulation of the magnetic field at 100 kHz and with amplitude = 2 G was applied to detect the absorption first derivative. The microwave power was kept at suitable low values (20 mW) to avoid saturation effects. The spin concentrations were determined by comparison of the sample ESR intensities with that of a standard DPPH (1,1 diphenyl-2picrylhydrazyl) sample containing 1.0066×10^{17} spins. The simulations of the ESR spectra were performed with the XSophe software (licensed by Bruker Biospin) using full matrix diagonalization. The effect of temperature was studied using a Bruker ESP 300E equipped with a ESR900 Oxford cryostat Traction mechanical experiments have been performed with a ZWICKI Z2.5/TN1S apparatus at a constant traction speed of 0.3 mm/min.

Results and Discussion

Fiber Generation and Characterization at Different Length Scales. The process of synthesizing fibers makes the use of an extrusion process where a vanadium oxide sol is expelled continuously from a syringe needle into a rotating baker containing a PVA−aniline solution (a and b in Figure 1). As explained and expressed elsewhere[17] the distance of the needle head from the external part of the rotating beaker is directly related with the imposed shear rate applied over the extruded sol. For this study, the applied shear rate is constant and equal to 235 s^{-1}. Final dried as-synthesized fibers can be seen in Figure 1c. We can notice that they are able to generate knots as a direct consequence of the fibers elasticity. Herein, the vanadium oxide sol is made of 50 wt % water and dimethylsulfoxide (DMSO). The same mixed solvent is used within the rotating beaker where both polyvinyl alcohol (PVA) and aniline have been dissolved (see experimental section for synthetic details). The strategy proposed here is to promote, as the vanadium oxide sol is extruded, a chemical reaction where the aniline is oxidized into poly aniline (PANI) and where the outer part of the vanadium oxide syringe out coming jet is reduced.

As already reported in the literature,[19] the intercalation of aniline within the V_2O_5 ribbons lamellae is followed by its oxidative polymerization into polyaniline, leading to V_2O_5−polyaniline conducting nanocomposites. The strongly oxidizing character of the vanadium oxide induces the aniline redox polymerization, thereby producing a p-doped inserted PANI within a n-doped mixed (V^{IV}/V^{V}) oxide host. Thus, in this process, a mutual doping takes place leading to a material with a double conduction mechanism. At this stage, this is certainly the first time that chemical reaction (mutual chemical redox reaction) is promoted while performing an extrusion process (physical chemistry aggregation process). The fibers macroscopic texture is proposed in Figure 2 as scanning electron microscopy (SEM) experiments.

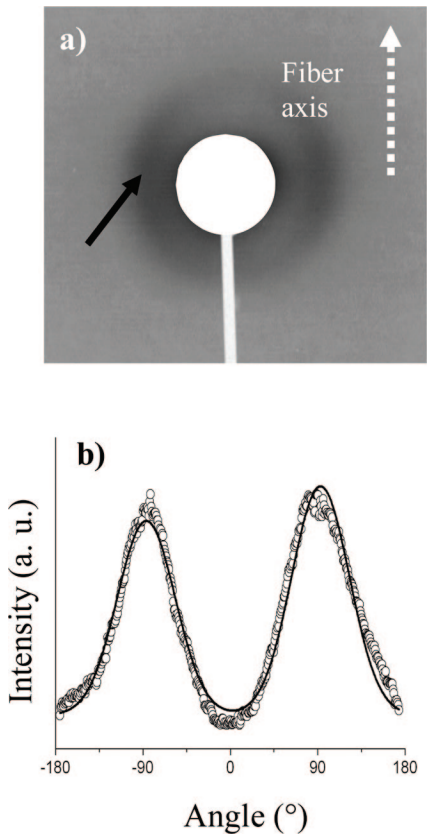

Figure 3. (a) Small-angle X-ray scattering pattern of a vanadium oxide fiber; the arrow points toward anisotropic scattering at $Q = 0.4$ Å^{-1}. (b) Angular variation of the intensity at $Q = 0.4$ Å^{-1}, the solid line is the result of a fit with Gaussian functions (HWHM $\approx 35°$).

Considering Figure 2a, we can observe that the fiber surface is very smooth with some submicrometric fibers bearing preferential oriental parallel to the fibers' main axis (Figure 2b). Also we can notice in Figure 2c that the fibers are not hollow and present a circular section. As usually observed,[16−18] the vanadium oxide nanoribbons preferential orientation, suggested by the Figure 2b, can be quantified with small-angle X-ray scattering experiments (SAXS) as shown in Figure 3. The broad signal at $Q \approx 0.4$ Å^{-1} (Figure 3a), which corresponds to a distance of 16 Å ($d = 2\pi$/Q), is characteristic of the inter-ribbon spacing, the ribbon thickness being about 1 nm.[19a,22] Its intensity is azimuthally modulated, which points toward preferential orientation of the ribbons.

As the intensity maxima is perpendicular to the fiber axis, it can be concluded that vanadium oxide ribbons are preferentially aligned along this axis. Radial scans in the fiber direction show no intensity modulation in this direction: statistically, all ribbons do have preferential orientations within the fiber. Intensity at $Q \approx 0.4$ Å^{-1} is reported as a function of the azimuthal angle in Figure 3b. Good fitting of the curve is obtained using Gaussian distributions with half-width at half maximum (HWHM) of about 35°. The distribution of ribbon orientations in real space can be deduced from these reciprocal space data, following the analysis developed for carbon nanotube fibers.[21c] It follows that the distribution of orientations of the ribbon long axes

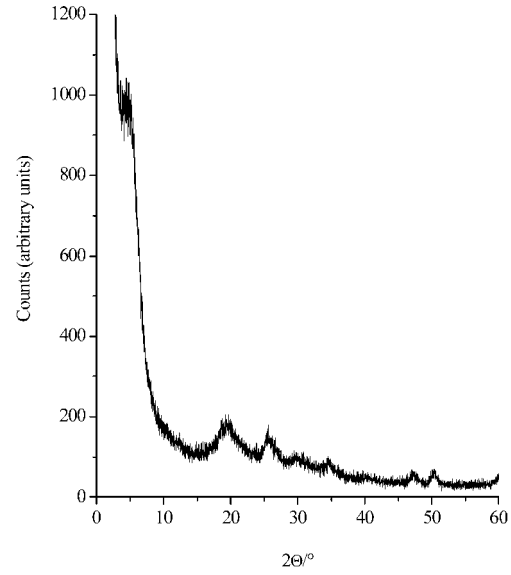

Figure 4. XRD pattern performed on PVA/PANI-V_2O_5 fibers.

corresponds to a Gaussian distribution with HWHM $\approx 30°$ in real space. This distribution width is almost double when compared with previous extrusion experiments under the same shear rate.[17] In the present case, the solvent in use is not only pure water, but a mixture of water/DMSO and furthermore, as discussed later in the text, the extrusion process is here addressed with a redox reaction (presence of aniline) that certainly perturbs the vanadium oxide nanoribbons alignment toward the fiber main axis. Consequently, the X-ray diffraction pattern (XRD) resolution is poor, revealing (Figure 4) a semicrystalline character of the as-synthesized fibers.

The XRD pattern is bearing a first broad 00 L diffraction peak (5.22°/2θ) that corresponds to a basal distance of 16.92Å. Therefore the interlayer expansion when compared with V_2O_5 xerogel is 5.45 Å, showing the intercalation of aniline within the V_2O_5 lamellae. This expansion is a little bit larger than the one observed previously by Kanatzidis et al.,[19] but in our case, because of the small amount of intercalated PANI (see later in the text), we certainly do have still water molecules present within the interlayer gallery. Also, a broad peak centered around 20° (2θ) (4.5 Å) is associated with the PVA chains organization, whereas we can distinguish sharp and weak peaks centered at 47° (2θ) (2.08 Å) and 51° (2θ) (1.98 Å) that might be indexed, respectively, to the reflection (2200) and (020) of the xerogel $V_2O_5 \cdot 1.8H_2O$.[22,23]

Because of the quite amorphous character of the fibers, the local environment of V^{5+} was investigated by ^{51}V magic-angle spinning nuclear magnetic resonance (^{51}V MAS NMR) spectroscopy. Unfortunately, the ^{51}V MAS NMR spectrum diplays a very broad signal covering almost 1500 ppm (not shown here). This poor resolution is certainly due to a large concentration of paramagnetic V^{4+} centers. A disorder in the material may also contribute to this line broadening. Therefore, these fibers were also investigated by electron spin

(22) Petkov, V.; Trikalitis, P. N.; Bozin, E. S.; Billinge, S. J. L.; Vogt, T.; Kanatzidis, M. G. *J. Am. Chem. Soc.* **2002**, *124*, 10157.

(23) (a) Yao, Y.; Oka, T.; Yamamoto, N. *J. Mater. Chem.* **1992**, *2*, 331. (b) Durupthy, O.; Steunou, N.; Coradin, T.; Maquet, J.; Bonhomme, C.; Livage, J. *J. Mater. Chem.* **2005**, *15*, 1090.

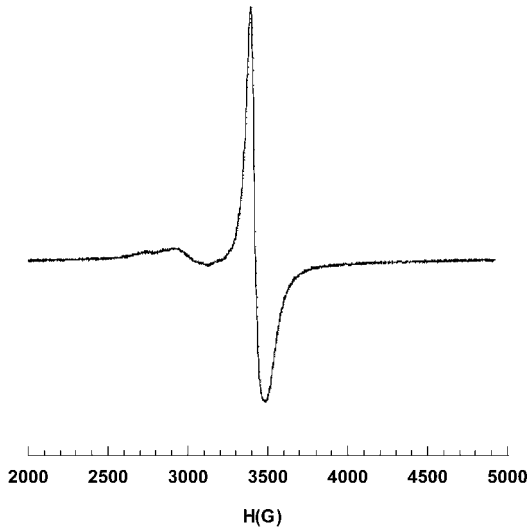

Figure 5. ESR spectrum of the PVA/V_2O_5 fibers recorded at room temperature.

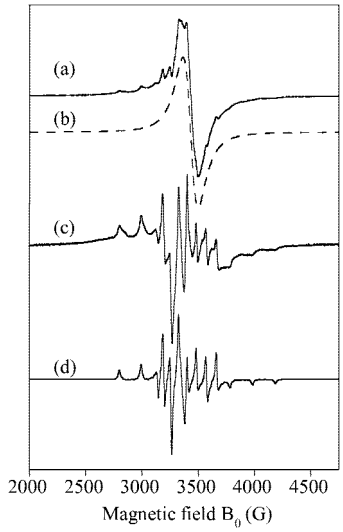

Figure 6. ESR spectrum of the PVA/PANI-V_2O_5 fibers recorded at room temperature. (a) Experimental spectrum. (b) Calculated background Lorentzian line with $g = 1.967$ and peak-to-peak line width = 135 G. (c) Spectrum of VO^{2+} obtained by substraction of the background line (b) from spectrum (a). (d) Calculated spectrum with parameters $g_{\|} = 1.930$, $g_{\perp} = 1.976$, $A_{\|} =$ 198 G, and $A_{\perp} = 74$ G.

resonance (ESR) spectroscopy. To compare the local environment of V^{4+} ions in the PVA/PANI-V_2O_5 fibers to that in the PVA/V_2O_5 fibers, we report the ESR spectrum of PVA/V_2O_5 fibers that were prepared by the extrusion process without aniline (Figure 5).

A single ESR line with peak-to-peak line width $\Delta B_{pp} \approx$ 95 G is observed at $g = 1.9701(9)$ for the PVA/V_2O_5 fibers, as previously reported.[17] The *g*-factor value is consistent with V^{4+} species. The hyperfine splitting due to the interaction with the ^{51}V nucleus ($I = 7/2$, 99.8% natural abundance) and the *g*-factor anisotropy are not observed in this spectrum. The reason is the occurrence of a narrowing phenomenon probably due to spin−spin exchange interactions between V^{4+} species, although an electron hopping process between V^{4+} and V^{5+} centers cannot be ruled out. In contrast, the ESR spectrum of the PVA/PANI-V_2O_5 fibers (Figure 6a) is different, suggesting a redistribution of the V^{4+} centers in the material upon polymerization of aniline in the fibers.

The ESR spectrum results from two superimposed signals. The first one (Figure 6b) is a broad structureless Lorentzian signal at $g \approx 1.967$ and with peak-to-peak line width $\Delta B_{pp} \approx 135$ G, corresponding to V^{4+} in exchange interactions or to an electron hopping process. Similar ESR spectra were previously reported for V_2O_5. nH_2O gels with a V^{4+}/V_T ($V_T = V^{5+} + V^{4+}$) ratio ranging from 3 to 15%.[12a,24−26] This exchange (or electron hopping) mechanism may be either due to a large amount of V^{4+} ions in the material or to a local concentration of V^{4+} centers that are not evenly distributed through the gel. Assuming the relative integrated areas of both spectra, it appears that the amount of V^{4+} species in PVA/PANI-V_2O_5 fibers is 3 times larger than that of in the PVA/V_2O_5 fibers. This may explain the poor resolution of the ^{51}V MAS NMR spectrum. This reduction of V^{5+} entities occurs certainly upon polymerization of aniline in the material. The second signal (Figure 6c) is best revealed when the signal of Figure 6b is substracted from the whole spectrum of Figure 6a. This signal is typical of isolated vanadyl VO^{2+} ions in an axial crystal field. The structure is due to the axial hyperfine interaction between the unpaired electron spin and the ^{51}V nuclear spin. Figure 6d shows the simulated spectrum with the following spin Hamiltonian parameters: $g_{\|} = 1.930^1$, $g_{\perp} = 1.976^1$, $A_{\|} = 198^2$ G, and $A_{\perp} = 74^2$ G. These parameters are also listed in Table 1 along with the ESR parameters from the literature for related materials, such as amorphous V_2O_5 (hydrated and dehydrated), $V_2O_5 \cdot nH_2O$ gels (hydrated and dehydrated), crystalline V_2O_5, and $[VO(H_2O)_5]^{2+}$. The ESR parameters for the PVA/PANI-V_2O_5 fibers are in fair agreement with those of $V_2O_5 \cdot nH_2O$ gels (see Table 1). In particular, the $g_{\|}$ value is close to that of an hydrated V_2O_5 gel. Actually, an hydration of V_2O_5 gels is generally associated to an increase in $g_{\|}$ (and to a less extent the $A_{\|}$ value).[12a,24−27] It suggests that the crystal fields around V^{4+} ions in PVA/PANI-V_2O_5 fibers are similar to that of $[VO(H_2O)_5]^{2+}$, which is a strongly distorted VO_6 octahedron with a short V−O bond along the *z* axis and a long V−OH_2 bond in trans position. The ESR signal of p-doped polyaniline could not be detected in the PVA/PANI-V_2O_5 fibers as was already observed for PANI−V_2O_5 nanocomposites.[19,28] Indeed, the ESR signal line width of polarons in PANI is particularly sensitive to the presence of other paramagnetic centers, as was examplified by the effect of paramagnetic O_2 on the ESR of the polarons in PANI.[29]

Indeed, the presence of paramagnetic species in the vicinity of the polarons induces interactions (wether magnetic dipolar or exchange), which broaden the ESR line of the polarons. In the case of PVA/PANI-V_2O_5 fibers, a spatial proximity

(24) Wiench, J. W.; Fontenot, C. J.; Woodworth, J. F.; Schrader, G. L.; Pruski, M.; Larsen, S. C *J. Phys. Chem. B.* **2005**, *109*, 1756.
(25) Luca, X.-V.; MacLachlan, D. J.; Bramley, R. *Phys. Chem. Chem. Phys.* **1999**, *1*, 2597.
(26) Babonneau, F.; Barboux, P.; Josien, F. A.; Livage, J. *J. Chim. Phys.* **1985**, *82*, 761.
(27) Nabavi, M.; Sanchez, C.; Livage, J *J. Philos. Mag., B* **1991**, *63*, 941.
(28) Guerra, E. M.; Brunello, C. A.; Graeff, C. F. O.; Oliveira, H. P. *J. Solid State Chem.* **2002**, *168*, 134–139.
(29) Houzé, E.; Nechtschein, M. *Phys. Rev. B* **1996**, *53*, 14309.

Table 1. ESR Parameters for Vanadium Oxide Compounds[a]

	$g_{\|}$	$g_{\perp}$	$A_{\|}$(G)	$A_{\perp}$(G)	ref
amorphous V_2O_5					
dehydrated	1.913	1.98	176	66	27
hydrated	1.932	1.977	198	74.5	27
V_2O_5 0.5 H_2O gel [b]	1.925	1.982	196	76	12a
V_2O_5 1.8 H_2O gel[b]	1.935	1.986	204	78	12a
V_2O_5 gel					
dehydrated,[c]	1.915 (1.926)	1.970(1.973)	193(194)	74.3 (73)	24[c] (25)[b]
hydrated,[c]	1.930(1.933)	1.990(1.973)	195(200)	74.5 (75)	24[c] ([24])[b]
crystalline V_2O_5	1.923	1.986	190	73	12a
$[VO(H_2O)_5]^{2+}$	1.934	1.987	203	66	12a
calcined V_2O_5/PVA/latex60% fibers	1.936[1]	1.976[1]	192[2]	71[2]	18
PVA/PANI-V_2O_5 fibers	1.930[1]	1.976[1]	198[2]	74[2]	this work

[a] The numbers in parentheses represent the standard deviation of the last digit. [b] Gel prepared by acidification of $NaVO_3$ with a proton exchange resin. [c] Gel prepared by dissolution of crystalline V_2O_5 with H_2O_2.

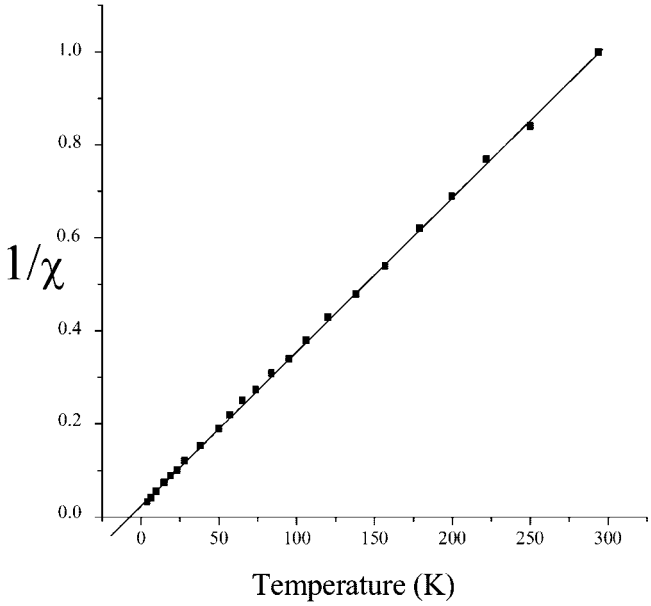

Figure 7. Evolutions of the as-synthesized fibers' reverse ESR susceptibility versus temperature.

between polarons of PANI and V^{4+} centers can therefore give rise to a similar line broadening effect. The amplitude of the ESR signal of the polarons is then strongly reduced to such a point that the signal becomes undetectable. Also, as observed in Figure 7, the fibers paramagnetic susceptibility evolution versus temperature is following a Curie−Weiss law addressed with a substantial antiferromagnetic contribution.

To complete this study, we have also performed magnetization measurements (Figure 8). Two kinds of measurements were made, either scanning the magnetic field at a given temperature or changing the temperature at a constant applied field. In both cases, the contribution of the sample holder has been deduced from the raw data to extract the sample magnetization. Let us first discuss temperature-dependent data obtained at a constant magnetic field. Similar results have been obtained at 2, 3, and 7 T. As an example, we will describe the data obtained at 2 T. After subtracting the contribution of the sample holder, the raw data have been used to deduce the magnetic susceptibility $\chi = M/H$ normalized per gram. These data are shown in Figure 8 from what the whole magnetic temperature behavior is discussed.

We have first plotted χT as a function of temperature. A linear regime with a negative slope is found above 100 K. The behavior reveals the presence of a temperature independent diamagnetic component. From the slope, we deduced $\chi_{dia} \approx -2.3 \times 10^{-7}$ emu cgs/g, which is consistent with orbital diamagnetism (typical values are about -5×10^{-7} emu cgs/g, but the presence of a very small amount of ferromagnetic impurities, certainly coming from the stainless steel syringe in used to extrude the acidic vanadium oxide gel, may account for the observed value). Between 50 and 100 K, the raw signal is close to zero (the sample and sample holder contributions almost compensate). As a consequence, a poor accuracy is obtained in this temperature domain. Below 40 K, the observed drop of the χT product suggests the occurrence of weak antiferromagnetic interactions. These interactions are better emphasized by the linear variation obtained when plotting $1/(\chi - \chi_{dia})$ versus T (Curie−Weiss plot). The deduced Curie−Weiss temperature is about −1.4 K (see inset of Figure 8), in total agreement with value estimated by Kanatzidis et al.[19b]

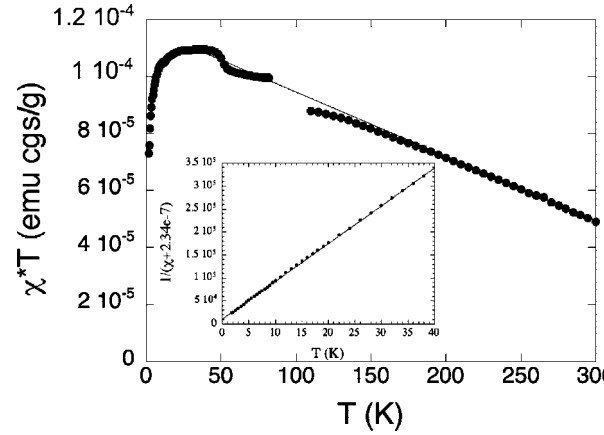

Figure 8. plot of χT versus T (χ is in emu cgs/g) showing the high temperature linear regime and the occurrence of antiferromagnetic interactions at low temperature. These interactions are emphasized by the Curie−Weiss plot ($1/(\chi - \chi_{dia})$ versus T) shown in inset.

To characterize the polyaniline, a Fourier transformed infrared (FTIR) spectrum on PVA/PANI-V_2O_5 fibers was recorded (Figure 9). All the vibration modes occurring below 1000 cm^{-1} can be attributed to the inorganic network.[19,30] More precisely, specific stretching modes of ν(V═O), $\nu(V_2O)$, and $\nu(V_3O)$ appear, respectively, at 1009, 762, and 489 cm^{-1} (broad); these peaks are characteristic of vanadium oxide hydrated gel.[23b] Also, a broad absorption from 3000

(30) Li, Z. F.; Ruckenstein, E. *Langmuir* **2002**, *18*, 6956.

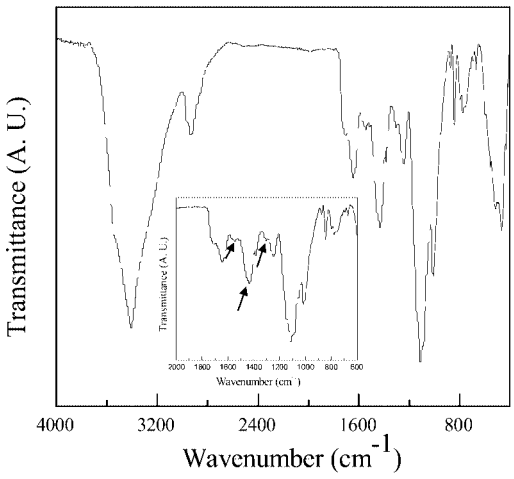

Figure 9. FTIR spectrum of PVA/PANI-V_2O_5 fibers. The embedded figure is focused on the wavenumber region 2000−600 cm^{-1} to blow up typical PANI normal vibration modes. The black arrows indicate specific PANI vibration modes.

to 3500 cm^{-1} is attributed to the stretching −OH modes arising both from water molecules and PVA. In this specific region, we can observe superimposed peaks or shoulders at 3505, 3407, and 3274 cm^{-1} that correspond to the N−H stretching modes.

Three peaks at 1560, 1450, and 1303 cm^{-1} can be distinguished and associated with the fibers' PANI counterpart (Figure 9 embedded, black arrows). First, two peaks at 1560 and 1303 cm^{-1} correspond, respectively, to the stretching vibration mode of benzenoid rings and the C−N stretching vibration of the secondary aromatic amine, respectively.[30] The third peak at 1450 cm^{-1} is slightly shifted when compared with the bulk emeraldine base of PANI (1500 cm^{-1}), indicating that the PANI may be present in the protonated, conductive state.[30] The FTIR results are in agreement with the oxidation of the aniline counterpart in PANI. To complete the fiber microstructure characterization, particularly concerning the hybrid fiber stoechiometry, we performed C, V, N elemental analyses. The following stoechiometry and associated elemental analyses have been found: (%C found, 29.5; calcd, 30.5); (%V found, 20.1; calcd, 21.7); (%N found, 0.8; calcd, 0.7), providing the following stoechiometry $(C_2H_4O)_{5.3}/(C_6H_5NH_2)_{0.22}V_2O_5 \cdot 1.9H_2O$. As previously found,[16−18] the fibers should be more regarded as a composite, because PVA represents around 49 wt % of the fiber core. Also, when considering previous bulk PANI-V_2O_5 xerogel,[19] we can notice that in our case, the amount of PANI present within the hybrid fibers is roughly divided per two, whereas the amount of water is increased by two. This specificity is important and the consequence is that in this case the organic conductive domains are certainly smaller than those obtained with bulk nanocomposite compounds.[19] This feature can certainly be explained by the fact that in the present study the redox reaction time between the vanadium oxide sol expelled from the syringe and the aniline present within the rotating beaker starting from the extrusion, up to the fiber removal from the beaker is quite short (typically less than 1 h), when compared with intercalation performed in bulk materials where samples are let to age between 5 and 24 h. Herein, to better characterize the organic conductive domains of PANI by ^{13}C MAS NMR while avoiding the presence of paramagnetic species, we have tried to dissolve the V_2O_5 host under basic conditions. Unfortunately, these composite fibers appear to be insoluble in water, even under strong basic conditions.

Fibers Sensing Properties toward Alcoholic Vapors. As claimed before, the intrinsic fiber shape offers the ability to construct conductive cells with a high degree of simplicity.[16] Also, the fiber section as well as the nanoribbon preferential orientation (and associated packing density) can be tuned playing with the shear rate applied during the extrusion process.[17,18] We previously demonstrated that the higher alignment of the nanoribbons subunits will permit us to obtain the higher sensitivity.[17,18] The fiber section can be measured using either optical microscopy or SEM (Figure 2c), and for a known fiber length, the sensing properties can be now quantitatively estimated with a conductivity measurement. The overall sensing properties are shown within Figure 10. First, considering Figure 10a, we can notice that the fibers are cycling. This feature is expected, as already observed with the first vanadium oxide fibers generated using the extrusion process mentioned herein.[16−18] The important issue, beyond cycling, is that the responses toward ethanol or butanol vapors source are not the same, as observed when considering the slope of the increasing conductivities under alcoholic vapor (Figure 10b). This particularity demonstrates that the new PVA/PANI-V_2O_5 oxide fibers are still selective toward sensing different alcohol vapors, when compared with our previous work.[16,18] The conductivity mechanism associated with the alcohol sensing effect has been hypothesized elsewhere in terms of surface charge electron-depletion strongly associated with the O−H bonds ionic character.[31]

Under alcohol vapors source, the alcohol can be adsorbed onto vanadium oxide ribbons by hydrogen bonds. Second, because of the ionic character of the OH group and its associated acidity (ethanol possesses a more acidic character than butanol), anionic charges are created at the outer ribbon subunits surface that promotes a statistical electrons release, i.e., conductive domains that grow to finally form the depletion layer.[16,31] Therefore, considering both the vapor tension and acidic character of OH group bearing, respectively, by the ethanol or butanol molecules it is obvious that the later alcohol will induce a slower kinetic of the conductivity evolution versus time exposure, promoting thus the observed selectivity (Figure 10b). Beyond cycling and selectivity properties, it is important to check for the fiber thermodynamic stability when exposed for long time above alcohol vapors, the result is proposed in Figure 10c. We can observe a first conductivity increase up to a maximum, followed with an abrupt loss of conductivity. As previously observed, this loss of conductivity is associated with a fiber color change from red to green, meaning that V^{5+} species are reduced to V^{4+}, creating thus a potential hole that diminishes the conductivity. When comparing this results with previous ones,[16−18] especially with inorganic fibers bearing nanoporosity,[18] the thermodynamic stability of the

(31) (a) Micocci, G.; Serra, A.; Tepore, A.; Capone, S.; Rella, R.; Siciliano, P. *J. Vac. Sci. Technol., A* **1997**, *15*, 34. (b) Liu, J.; Wang, X.; Peng, Q.; Li, Y. *Adv. Mater.* **2005**, *17*, 764.

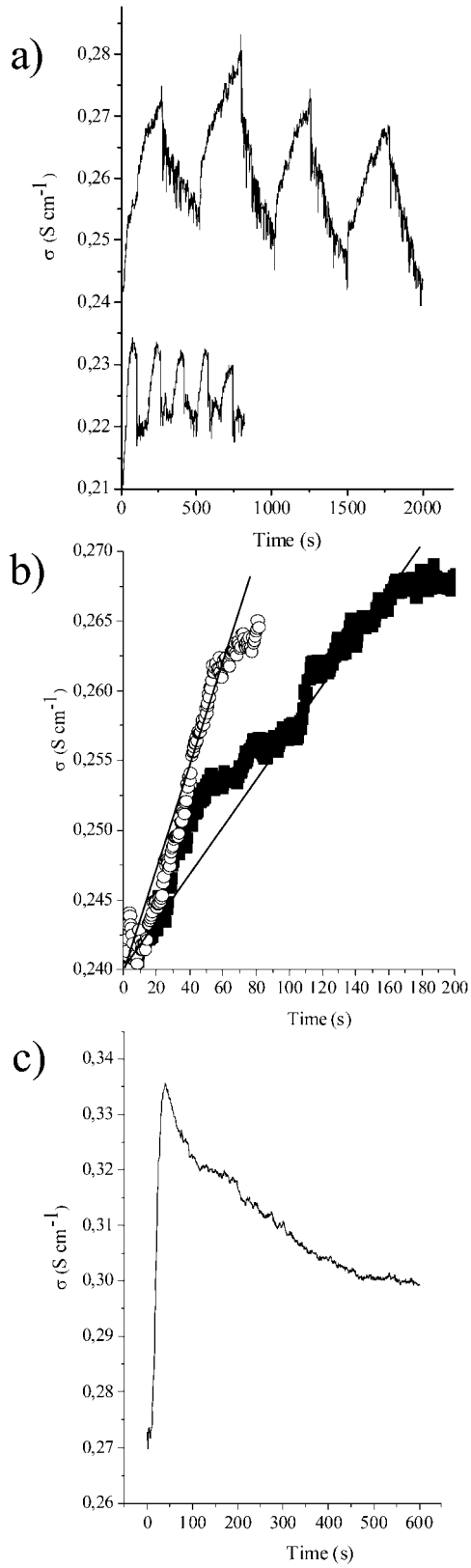

Figure 10. Sensing properties of PVA/PANI-V_2O_5 fibers. (a) Fibers cycling abilities upon butanol (top) and methanol (down) alcoholic vapors; (b) zoom over the increasing conductivities when fibers are positioned above alcoholic vapor,○ ethanol, ■ butanol (the butanol curve has been translated down to help comparing the curves slope, plain line); (c) evolution with time of the vanadium oxide fibers conductivity profiles at 42 °C when placed above a beaker containing pure ethanol. The results have always been obtained for a single vanadium oxide fiber constituting the conductive cell.

fibers presented herein has been lowered, mainly for two reasons. First, because of the aniline/V_2O_5 redox reaction, the concentration of V^{4+} species has been enhanced, as discussed within the ESR section. Second, these fibers do not possess any induced porosity, and thus when all the V^{5+} present at the fiber outer part is completely reduced, the surface conductivity is drastically damaged, without any sublayer conductive domains compensation that have been shown to be induced by promoting nanoporosity.[18] Also, considering these fibers' sensitivity, they are able to detect 5 ppm of ethanol within 3−5 s, with 35 s to reach 90% of the maximal conductivity value. This sensitivity at 42 °C is lower when compared to pure inorganic nanoporous vanadium oxide fibers where, for instance, the best sensitivity allows sensing down to 0.1 ppm of ethanol within 3−5 s at 42 °C.[18] Also, when sensing, we can notice herein that the increase of conductivity is low, varying only the second decimal placed on the conductivity scale. This was not the case with previous work[16−18] where the sensing performance took place with 1 or 2 orders of magnitude over the conductivity measurements. Herein, the PVA/PANI-V_2O_5 fibers are bearing a bimodal conductivity due to the p-doped conducting polyaniline inserted into a n-doped vanadium oxide host matrix. As a direct consequence, the intrinsic starting fibers' conductivity (without alcohol vapors) is higher than the PVA/V_2O_5 and the pure inorganic ones. As ascribed with ESR quantitative measurements, the redox intercalation of aniline is associated with a strong reduction of the V^{5+} species into V^{4+} ones. Considering this issue, and as the vanadium oxide fibers' sensing property is based on the oxidation of alcohol into aldehyde upon reduction of V^{5+} species into V^{4+} ones,[31,18] the potential of V^{5+} species of being reduced through alcohol vapors is thereby strongly minimized, diminishing thus both the sensitivity and the amplitude of the conductivity's increase when sensing alcohol vapors. On the other hand, we have to bear in mind that the pure inorganic nanoporous fibers were extremely fragile[18] mechanically. This is not the case with the fibers presented herein, as discussed below in the text.

Fiber Mechanical Properties. The mechanical properties of the PVA/PANI-V_2O_5 are strongly different from those of PVA/V_2O_5 fibers (Figure 11). The PVA/V_2O_5 fibers possess both a short elastic regime associated without any plastic regime. As a direct consequence, the Young modulus is quite high 22 GPa with a weak strain before breaking (Table 2). When introducing PANI through the generation of the PVA/PANI-V_2O_5 fibers, we can see in Figure 10 that the toughness, which is represented at first glance by the surface area under the traction curves, is tremendously increased. The PVA/PANI-V_2O_5 traction curve bears a strong plastic regime allowing a strain under traction of around 7%. This feature allows the fibers to reach a toughness of 12 J g^{-1}, six times higher than fibers obtained without PANI (Table 2).

When comparing the PVA/PANI-V_2O_5 fibers' toughness with inorganic macroporous fibers, the toughness value has been increased by more than 120 times. On the other hand, as the direct consequence of the enhanced toughness the Young modulus is decreased to 3.4 GPa (Table 2).

The enhanced toughness bearing by the PVA/PANI-V_2O_5 fibers may be due to the fact that PANI is disrupting the

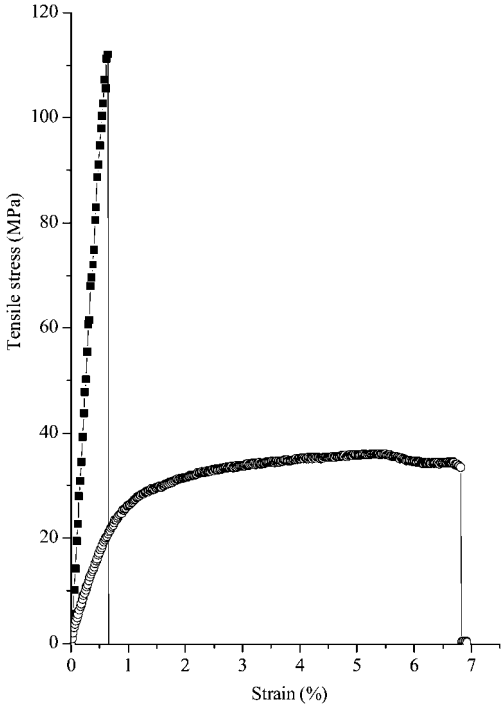

Figure 11. Fiber mechanical properties. Measurements were performed at a strain rate of 0.3 mm min^{-1}. ■,PVA/V_2O_5 fibers, ○, $PVA/PANI\text{-}V_2O_5$ fibers. The fibers were generated using the same shear rate of 235 s^{-1}.

Table 2. Mechanical Characteristics for the Vanadium Oxide Fibers Generated under the Same Shear Rate (235 s^{-1})[a]

fiber types	E (GPa)	σ_R (Mpa)	$\varepsilon_{breaking}$ (%)	ϵ_{max}	T (J g^{-1})
PVA/V_2O_5[b]	22	125	0.73	0.73	2
$PVA/PANI\ V_2O_5$	3.4	34	7	7	12
nanoporous V_2O_5[c]	4	5	0.2	0.2	<0.1

[a] Measurements were performed at a strain rate of 0.3 mm/min. E is the Young's modulus, σ and ϵ represent, respectively, the stress and strain before breaking. [b] Data mainly extracted from ref 16. [c] Data mainly extracted from ref 18 for inorganic nanoporous vanadium oxide fibers generated from 10% weight latex particles.

hydrogen bounds between PVA and surface V−OH pending groups, affecting thus the fiber axial cohesion under traction. This effect optimizes the ability of the nanoribbons subunits to stack-slip on each other, thereby enhancing the fiber's axial plasticity while, on the other hand, minimizing the obtained Young modulus (elasticity).

Conclusion

For the first time, $PVA/PANI\text{-}V_2O_5$ composites have been generated bearing organization at the mesoscopic and macroscopic length scales as obtained through a redox extrusion process. Also, considering the extrusion process itself, this is certainly the first time that a redox reaction is addressed while performing an extrusion process. The fibers have been characterized at different length scales, revealing a 30° preferential orientation of the nanoribbons subunits toward the macroscopic fiber main axis. At the microscopic length scale, despite a semiamorphous nature, ESR spectroscopy shows a strong reduction of V^{5+} species to V^{4+} paramagnetic centers and reveals that the local environment of V^{4+} is close to hydrated vanadium oxide xerogels. Concerning the organic counterpart, both ESR, FTIR as well as the fibers' intrinsic conductivity suggest that the aniline is oxidized into PANI. These new $PVA/PANI\text{-}V_2O_5$ fibers are cycling while still sensing alcoholic vapors and offering a good selectivity. The addressed sensitivity allows sensing of 5 ppm ethanol within 3−5 s at 42 °C, which is lower than that obtained with inorganic nanoporous vanadium oxide fibers, but higher still than highest results observed for non-fiber-based materials.[31] Beyond this, the as-synthesized $PVA/PANI\text{-}V_2O_5$ macroscopic fibers possess a toughness of 12 J g^{-1}, a value six times higher when compared with PVA/V_2O_5 fibers[16,17] and a factor higher than 120 when compared with nanoporous inorganic fibers.[18] Overall, the use of a redox reaction to promote new $PVA/PANI\text{-}V_2O_5$ fibers allows a gain of toughness and fibers' intrinsic conductivity but a loss of sensitivity, meaning again that the parameters involved within the fibers'sensing and mechanical properties are acting in a strong partitioning mode rather than a cooperative one. The next step will be to include multiwall carbon nanotubes within the starting vanadium oxide sol with a guess to promote both the fibers' sensing and mechanical properties. This work is under progress and will be published in due time.

Also, we found out that these fibers are insoluble in water, even under basic conditions, offering thus the potentiality to use these fibers bearing a good conductivity not as sensors, but rather as electrodes.

Acknowledgment. This work is part of the FAME-MIOH European network of exellence. We acknowledge the "Ile de France" region for financial support that concerns the ESR Bruker Elexsys E500 spectrometer acquisition (Grant E.1663). R.B. thanks Dr. P. Poulin for helpful discussion concerning the fibers' toughness calculation.

CM800886V